Technical Paper

大 韓 造 船 學 會 誌
第25卷 第4號 1988年 12月
Journal of the Society of
Naval Architects of Korea
Vol. 25, No. 4, December 1988

Some Applications of the TUMMAC Method to 3D Water-wave Problems

by

Young-Gill Lee*, Hideaki Miyata** and Hisashi Kajitani**

TUMMAC差分法에 의한 3次元 非線形波의 解析에 관한 硏究

李永吉*, 宮田 秀明**, 梶谷 尙**

Abstract

Two versions of the TUMMAC(Tokyo University Modified Marker-And-Cell) method, i.e., TUMMAC-IV$_{vm1}$ and TUMMAC-VI are applied to two water-wave problems.

The ship wave of a Series 60 model (C_B=0.6) and of the fore-body of a HSVA tanker model are simulated by the TUMMAC-IV$_{vm1}$ method and the results are compared with the experimental results. From the comparison with the experimental data it is ascertained that the TUMMAC-IV$_{vm1}$ method is useful for the analysis of the characteristics of nonlinear ship waves.

Three-dimensional wave breaking is realized by the TUMMAC-VI method in the simulation of a flow about a vertical rectangular cylinder. From the results of this simulation, it is shown that the TUMMAC-VI method is very available for the simulation of 3-dimensional wave breaking phenomena.

요 약

TUMMAC差分法이 두 가지의 三次元波, 즉 배의 航走에 따른 波形과 垂直四角柱 주위의 碎波解析에 適用되어졌다.

Series 60 (C_B=0.6) 模型船과 HSVA 模型船의 船首部에 의한 波形이 自由表面과 船體後半部에서의 boundary cell 처리를 엄밀화한 TUMMAC-IV$_{vm1}$方法에 의하여 計算되어졌으며, 그 결과가 實際의 實驗結果들과 比較되었다. 實驗結果와의 비교를 통하여, TUMMAC-IV$_{vm1}$方法은 배에 의한 非線形波의 特性解析에 매우 應用性이 높음을 보였다. 특히, 肥大船型인 HSVA 模型船의 경우는 計算된 非線形船首波의 特性이 實驗結果와 좋은 일치를 보였다.

垂直四角柱주위의 碎波를 포함한 심한 非線形波가 三次元非線形波의 對表的인 例로써 TUMMAC-VI方法에 의하여 計算되었다. TUMMAC-VI方法은 二層流를 함께 푸는 方法으로, 두가지 流體 사이의 密度變化, 즉 marker-density를 이용하여 interface를 결정하게 된다. 그러나, 非壓縮性流體에 관한 N-S 方程式의 解이므로, 그 밖의 計算에서는 각각의 對表的인 密度를 사용한다. 計算結果는

本 論文은 1987年度 大韓造船學會 秋季硏究發表會에서 發表된 論文임
Manuscript received: April 4, 1988, revised manuscript received: August 22, 1988

* Member, Graduate School, Department of Naval Architecture, The University of Tokyo, Japan
** Department of Naval Architecture, The University of Tokyo, Japan

四角柱 앞부분의 圓形波와 앞어깨에서의 심한 경사를 가지는 波, 뒷부분에서의 複雜한 碎波現像들이 실제의 波特性을 잘 나타내어 주었다. TUMMAC-Ⅵ方法은 interface의 처리를 포함하여 앞으로도 改善의 여지가 많으며, 단지 空氣와 물만이 아닌 一般的인 二層流의 해석에도 폭 넓게 이용될 수 있으리라 본다.

1. Introduction

A finite difference method (FDM) is very powerful method for the simulation of nonlinear hydrodynamic phenomena, since it directly solves the Navier-Stokes (NS) equations in a finite-difference form by time-marching until a steady state is reached. Nowadays attentions have been focused on the nonlinear wave phenomena in ships and offshore structures, and these problems can be more thoroughly solved by the FDM.

A FDM for the problems of the ship and offshore structure waves and its applications have been developed at the Experimental Towing Tank of the University of Tokyo since 1979[1-10]. It is called TUMMAC-method, because its basic algorithm is same with the MAC-method[11].

TUMMAC-IV[9, 10] is the version for the simulation of waves around an arbitrary three-dimensional hull form. The hull surface is approximated by simplifying the water-line into a successive segments and the frame-line into step-like configuration, and a free-slip condition is applied on the body boundary. To raise the computational accuracy, the improved version TUMMAC-IV$_{vm1}$ employs a variable mesh system in vertical direction.

In this paper, the TUMMAC-IV$_{vm1}$ is improved so as to compute the waves of the full-length of a ship model by modifying the velocity extrapolation method in the body boundary cell of aft-body, by giving the exact value of relaxation factor ω_f in the pressure computation of a body boundary cell that contains a free surface and by modifying free surface treatment that uses the Lagrangian movement of marker particles. The usefulness of the improved version of the TUMMAC-IV$_{vm1}$ method is demonstrated by the simulation of the waves generated by Series 60 and HSVA models.

It is difficult to explain the 3-dimensional wave breaking phenomena by the previous TUMMAC-method[9, 10], although the 2D wave breaking simulation method is developed by Miyata[12]. Therefore, a new version TUMMA-VI[13] which can deal with the 3D wave breaking phenomena in two-layer flows is developed. In the previous works, the Lagrangian movement of markers is used for the computation of free surface configuration, but the values of marker-density on the pressure point of each cell are used in the TUMMAC-VI method. The availability of this method is demonstrated by the simulation of 3-dimensional breaking waves about a vertical rectangular cylinder piercing the air-water interface.

2. TUMMAC-IV$_{vm1}$ Method

2.1. Brief discription of the method

The details of the TUMMAC-IV$_{vm1}$ method are explained in reference[9], so the computational procedure is described here very briefly.

The nonlinear ship-wave problem is solved by computing the flow field around a ship. Therefore, the continuity equation and *NS* equations are governing equations. However, since inviscid boundary conditions are imposed on the free surface and body surface, in reality the Euler equations are used.

The basic concept of the solution algorithm is similar to the MAC-method of Welch et al.[11] and Hirt & Nichols[14]. By solving the Poisson equation derived from the continuity and *NS* equations as a boundary-value problem, the velocity field is updated from the new pressure field. Then, the marker particles are moved in the Lagrangian manner with the new velocities, and these new locations give the new configuration of the free surface. The pressure on the center of each cell is calculated by the Poisson equation under the new velocities and the

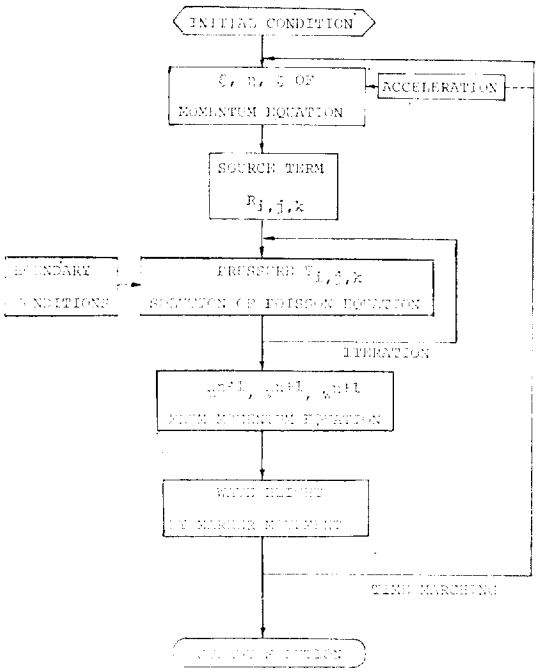

Fig. 1 Block diagram of the TMMAC-IV scheme

free-surface. The cycle is repeated until steady state is attained. The computational procedure is shown in Fig. 1.

A cartesian coordinate system is employed, in which the x-axis is the centerline on the waterplane of a ship. The y-axis is oriented transversely, and the z-axis is oriented vertically, positive upward. The ship advances in the negative x-direction. A staggered semi-variable mesh system is used, and

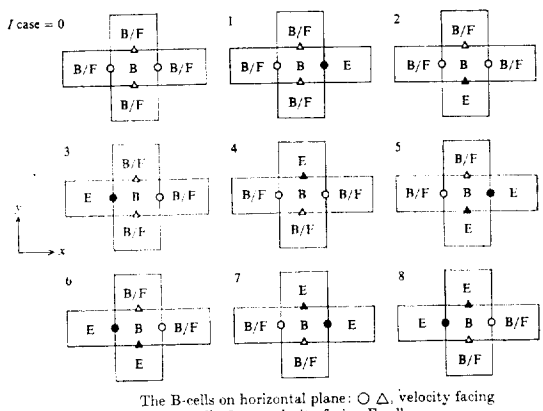

Fig. 2 Boundary-cells on horizontal plane

the dimensions of each rectangular cell are DX, DY and $DZ(k)$.

The NS equations are represented in a finite-difference form by forward differencing in time and centered differencing in space except for the convective terms. The differencing of the convective terms are described by a hybrid scheme that is a combination of a second-order centered differencing and a second-order upstream differencing (donor-cell method). For instance, the first term of the x-directional convective term is written as equation (1).

$$\frac{u^2_{i+1,j,k}-u^2_{i,j,k}}{DX}=\frac{1}{4DX}\{(u_{i+1/2,j,k}+u_{i+3/2,j,k})^2-(u_{i-1/2,j,k}+u_{i+1/2,j,k})^2\}+\alpha\{|u_{i+1/2,j,k}+u_{i+3/2,j,k}|\cdot(u_{i+1/2,j,k}-u_{i+3/2,j,k})-|u_{i-1/2,j,k}+u_{i+1/2,j,k}|(u_{i-1/2,j,k}-u_{i+1/2,j,k})\}\quad(1)$$

Here, α is a combination factor. Namely, $\alpha=0$ is precisely the centered differencing, and $\alpha=1$ is precisely the donor-cell method. In this case, the time stability requirement of Euler equations is $\alpha\geq \max(|\bar{u}|\cdot DT/DX,\ |\bar{v}|\cdot DT/DY,\ |\bar{w}|\cdot DT/DZ)$ from the Hirt's stability analysis and the courant number. Then $\bar{u}, \bar{v}$ and $\bar{w}$ are the convective velocity components.

All the cells are classified into fluid cells (F-cells), body boundary cells (B-cells) and empty cells (E-cells) as shown in Fig. 2. The hull surface is made of waterlines and framelines. The former is approximated by a succession of straight segments, and the vertical variation within each cell is ignored for the latter[9]. A free-slip body boundary condition is fulfilled in the body boundary cells. Then each B-cell is classified into the nine horizontal cases as shown in Fig. 2. With the vertical cases[9], the total number of cases is thirty-five.

A free-slip condition must fulfil (1) that the velocity normal to a body surface is zero, (2) that the tangential velocity does not have normal gradient, and (3) that the divergence of a B-cell is zero. Under these conditions, the pressure of a cell must be satisfied with the pressure condition as equation (2).

$$\phi_{i,j,k}^{m+1}=\phi_{i,j,k}^{m}-\frac{\omega}{2\delta DT}(\vec{V}_p\cdot\vec{n}) \quad (2)$$

where,

$$\delta=\frac{1}{DX^2}+\frac{1}{DY^2}+\frac{1}{\{DZ(k)\}^2}$$

Here, $\vec{V}_p$ and $\vec{n}$ are the fluid velocity vector at the center of a segment and a unit outward normal vector of a segment respectively, m is the number of time step, and ω is a relaxation factor.

On the free surface, the Lagrangian movement of marker particles is used for the fulfilment of kinematic condition, and the "irregular star" technique of Chan & Street[15] is used for the dynamic condition. In this study, four markers are used instead of one marker in each cell, after the movement of markers the wave height of the center of a cell is determined by the interpolation of the closest three marker points. The reason for using this method, in the case of low speed ship, is that the sign of velocity is very rapidly changed on the free surface after the acceleration of the flow.

In the present method, the conditions of centerplane, inflow, bottom, side and outflow boundaries are same with those in Miyata, et al.[9].

2.2. Improved implementation of body boundary condition

In the present study, the first improvement is that the relaxation factor ω_f is exactly reduced by the 3-dimensional treatment of a boundary cell containing the free surface, shown in Fig. 3. The reduced

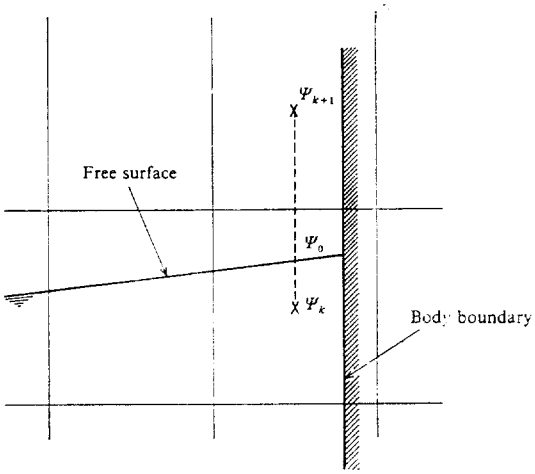

Fig. 3. Definition sketch for the treatment of a boundary cell containing a free surface

ω_f is derived as equation(3).

$$\omega_f=\frac{A\cdot\{DZ(k)\}^2\cdot\omega}{A\cdot\{DZ(k)\}^2-(1-\eta)\cdot\omega} \quad (3)$$

where,

$$A=2\left[\frac{1}{DX^2}+\frac{1}{DY^2}+\frac{1}{\{DZ(k)\}^2}\right]$$

$$\eta=(Z_{k+1}-Z_k)/(Z_{F.S.}-Z_k)$$

The second improvement is the extrapolation method of velocity w in a B-cell of the aft-body. In the case of ICASE=2, 3 and 6 (with KCASE=1, 2 [9]) as shown in Fig. 2, the velocity w of a B-cell is extrapolated from the vertical velocities of one

Table 1 Condition of computation for Series 60

Condition of hull		Fore-body	Full-length of hull
Domain of computation (m)	Length	1.152	5.015
	Breadth	0.496	0.600
	Depth	0.369	0.314
Cell size (m)	DX	12.0	17.0
	DY	8.0	15.0
	DZ	7.41～39.15	6.65～40.90
Approximate number of used cell		137000	236000
Time increment DT (s)		0.00329 0.00230 0.00197	0.00572
Time steps for acceleration		400 200 200	300
Total time steps		600 400 400	500
Combination factor α		0.5	0.5
Relaxation factor ω		1.5	1.5
Kinematic viscosity ν (m^2/s)		0.0	0.0
Froude number Fn		0.18 0.25 0.30	0.18
Speed of advance(m/s)		0.891 1.238 1.485	0.891
Length of ship model (m)		0.90	2.50

outer and one after F-cells, shown in equation(4).

$$w_{i,j,k}=w_{i+1,j,k}\cdot SST+w_{i,j-1,k}\cdot(1-SST) \quad (4)$$

where,

$$SST=\sin^2\{\mathrm{Tan}^{-1}(DY/DX)\}$$

3. Computed Results by TUMMAC-IV$_{vm1}$

3.1. Condition of computation

The computations of waves generated by the fore-body and full-length of the Series 60 (C_B=0.6), 4210W ship model of 2.5m length case are performed. The conditions of computation are shown in Table 1. Figure 4 shows the cell division of the Series 60 hull on a (y,z)-vertical plane at I=138. The vertical spacing $DZ(k)$ is constant above the free surface of the rest condition, and it varies from 6.65 to 40.9mm beneath it.

The computations are performed at the speeds of Fn=0.18, 0.25 and 0.30 for the fore-body, at the Fn=0.18 for the full-length. The total number of cell is about 236,000 for the full-length case using the computer memory of 19.2MB. The CPU time is about 1.8 hours using HITAC M-680H of the University of Tokyo for the 500 time steps (full-length, Fn=0.18).

Moreover, the computations of waves generated by the fore-body of the HSVA model of 7.6m long are performed. The purpose of this computations is to simulate the nonlinear bow wave phenomena about a hull form with blunt bow. The chosen Froude numbers are 0.15 and 0.17.

3.2. Computed results and comparison

The simulation of the waves by the fore-part of the Series 60 model at three Froude numbers is executed in one computational job. Consequently, three wave-contour maps at steady states at Fn= 0.18 (600-th step), 0.25 (1000-th step) and 0.30 (1400-th step) are as shown in Fig. 5. The angles of wave-crest-line of the bow waves are decreased by the increasing Froude number. It shows fine agreement with the one of the distinctive characteristics of the nonlinear bow waves. Figure 6 shows the wave profiles along the hull surface. The agreement with experimental results is improved with the

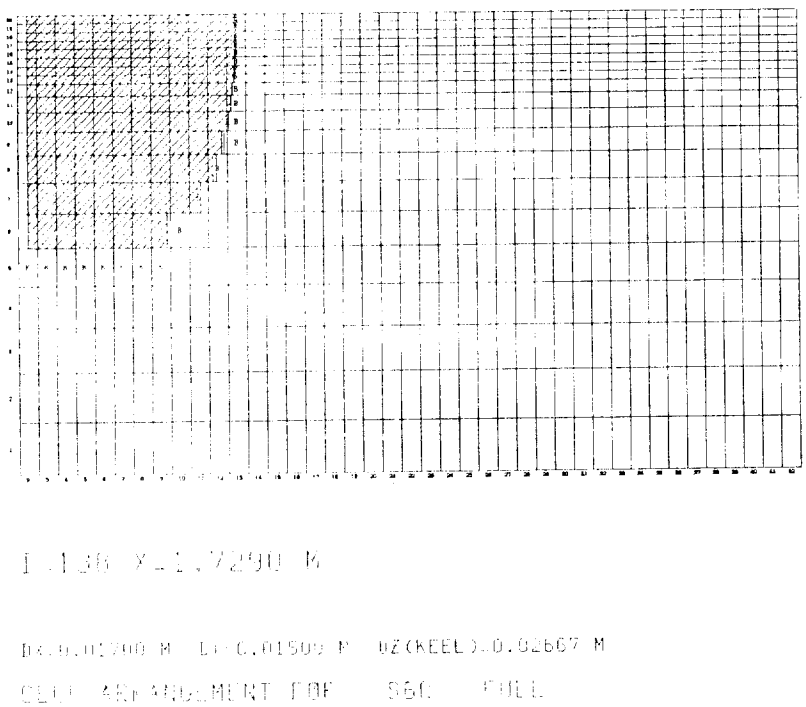

Fig. 4 Cell division of a Series 60 ship model on a (y,z)-vertical plane

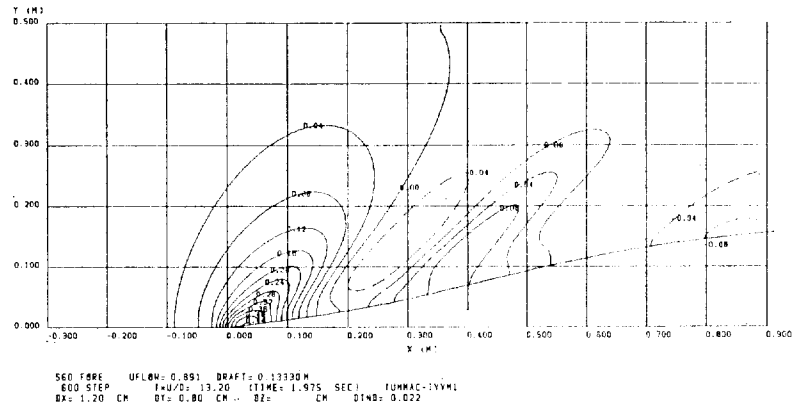

Fn=0.18

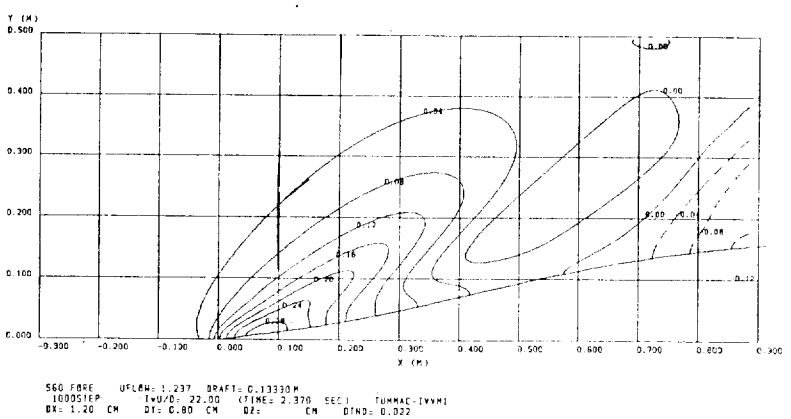

Fn=0.25

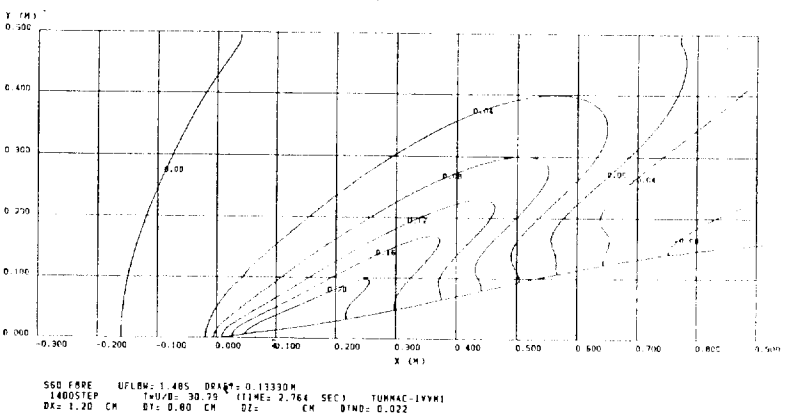

Fn=0.30

Fig. 5 Computed wave-contour maps of the forebody of a Series 60 ship model at Fn=0.18, 0.25 and 0.30

increase of Froude number.

Figure 7 shows the wave-contours around the full-length of the Series 60 model at $Fn=0.18$ (500-th step). These are good results except that it shows dimpled wave-contour in the region near the midship. The dimpled contour may be due to the very rapid change of the sign of velocity on the free surface. The computed wave profile on the body surface of full-length is compared with measurements in Fig. 8. The agreement with the measurements is good, especially on the surface of the aft-body rather than the fore-body. It seems that the cell size is not sufficiently fine on the fore-body surface, despite that the water line of the Series 60 model has very sharp end as well as delicate curve on the fore-body.

The perspective views of computed wave configuration around the fore part of the HSVA model at $Fn=0.15$, 0.17 (600-th step) are shown in Fig. 9. In the speed range from $Fn=0.15$ to 0.17 the wave resistance of the HSVA model increases very rapidly. This phenomenon of the abrupt increase of wave resistance is attributed to the conspicuous wave formation near the shoulder at $Fn=0.17$ which shows a remarkable difference from $Fn=0.15$ as observed

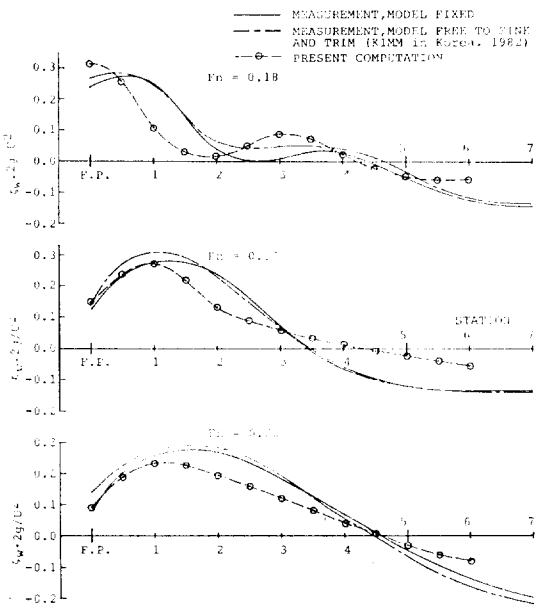

Fig. 6 Comparison of wave profiles on the hull surface of the forebody of a Series 60 ship model at $Fn=0.18$, 0.25 and 0.30

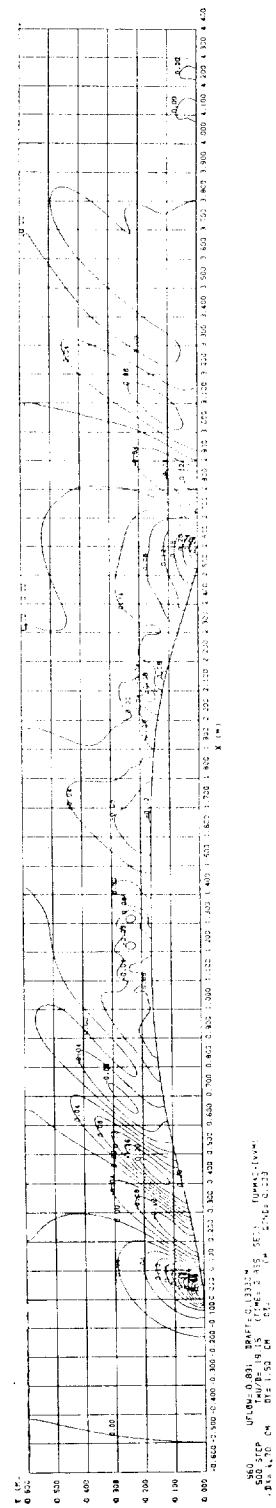

Fig. 7 Computed wave-contour map of the full length of a Series 60 ship model at $Fn=0.18$, steady state at the 500th time step, the uniform stream is accelerated for 300 time steps

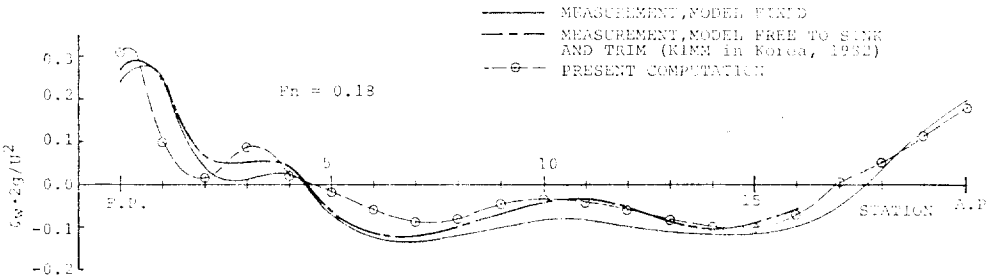

Fig. 8 Comparison of wave profiles of the full length of a Series 60 ship model at $Fn=0.18$

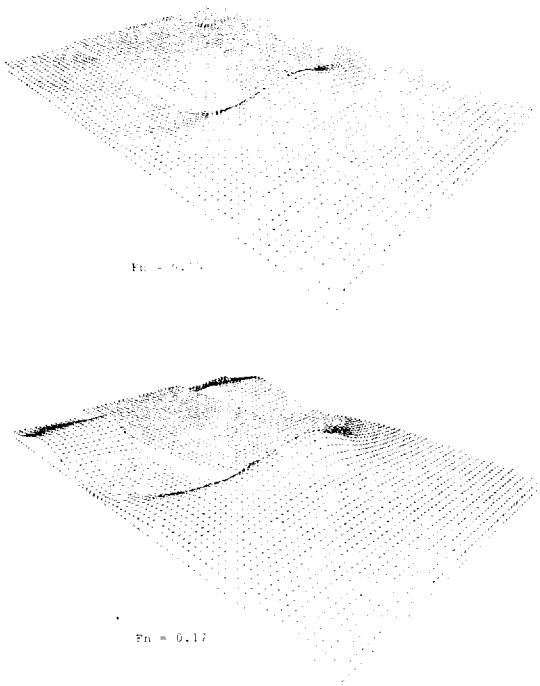

Fig. 9 Perspective views of waves around the fore-body of a HSVA model at $Fn=0.15$, 0.17, 600th time step

in Fig. 9. This is also noted in Fig. 10 for the wave-contour, in which the wave formations near the bow do not show substantial difference between two Froude numbers. The computed wave profile along the hull surface is compared with measurements in Fig. 11 together with the computed wave profile by the original Rankine source method by Gadd(1979). It must be noted that this method and the TUMMAC -IV method employ nonlinear free-surface conditions and no others. The superior accuracy of the present method is obviously shown, especially near the shoulder.

4. TUMMAC-VI Method

4.1. Brief description of the method

The incompressible two-layer flow is considered. Then the continuity equation and *NS* equations are employed as governing equations[13]. Therefore, the density of the fluid is assumed to be constant within each fluid region.

The basic concept of the algorithm is same with the former TUMMAC-method. Namely, the Cartesian coordinate system in the staggered semi-variable mesh system is used, and the *NS* equations are represented in a finite-difference form by forward differencing in time and centered differencing in space except for the convective terms. The differencing of the convective terms are described by the donor-cell method.

The computational procedure is shown in Fig. 12. The marker-density distribution is calculated from the kinematic free-surface condition of interface. For the calculation of the marker-density, Adams-Bashforth method is employed in time-differencing, and second-order centered differencing for the space-differencing as shown in equation(5, 6).

$$\rho_m^{n+1}=\rho_m^n+\left(\frac{3}{2}V^n-\frac{1}{2}V^{n-1}\right)\cdot DT \tag{5}$$

where,

$$V=-\left(\frac{u_{i-1/2,j,k}+u_{i+1/2,j,k}}{2}\cdot\frac{\rho_{mi+1,j,k}-\rho_{mi-1,j,k}}{2DX}+\frac{v_{i,j-1/2,k}+v_{i,j+1/2,k}}{2}\cdot\frac{\rho_{mi,j+1,k}-\rho_{mi,j-1,k}}{2DY}+\frac{w_{i,j,k-1/2}+w_{i,j,k+1/2}}{2}\cdot\frac{\rho_{mi,j,k+1}-\rho_{mi,j,k-1}}{2DZ(k)}\right) \tag{6}$$

The Poisson equation for the respective layers are independently solved. The pressure field of the layer -2 is determined after that of the layer-1 is determined.

The no-slip body boundary condition is approximately implemented on the body surface. The velocities on the body surfaces are set at zero, and other velocities of a boundary cell are extrapolated into the body so that the velocities are zero on the body surface and the continuity condition of the B-cells is satisfied. Since a rectangular cylinder is chosen as an obstacle in this study, two extrapolated values of velocity are given on one velocity point inside the corner and one of the two in the related direction is used for the computation of the convective and diffusive terms. Pressure is also extrapolated from fluid to body making use of the relation of the momentum equation.

Velocities for an uniform stream or oscillatory flow are given on the inflow boundary. The pressure

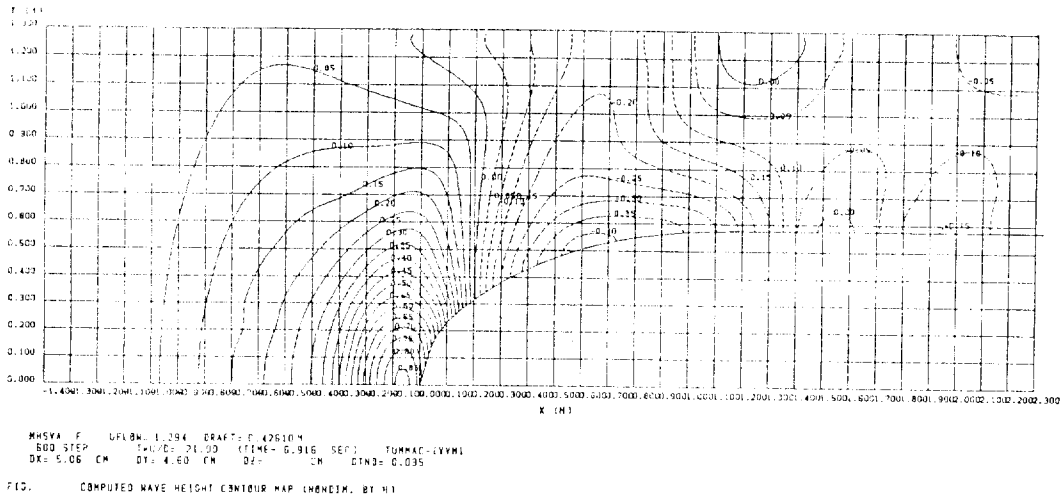

Fn = 0.15

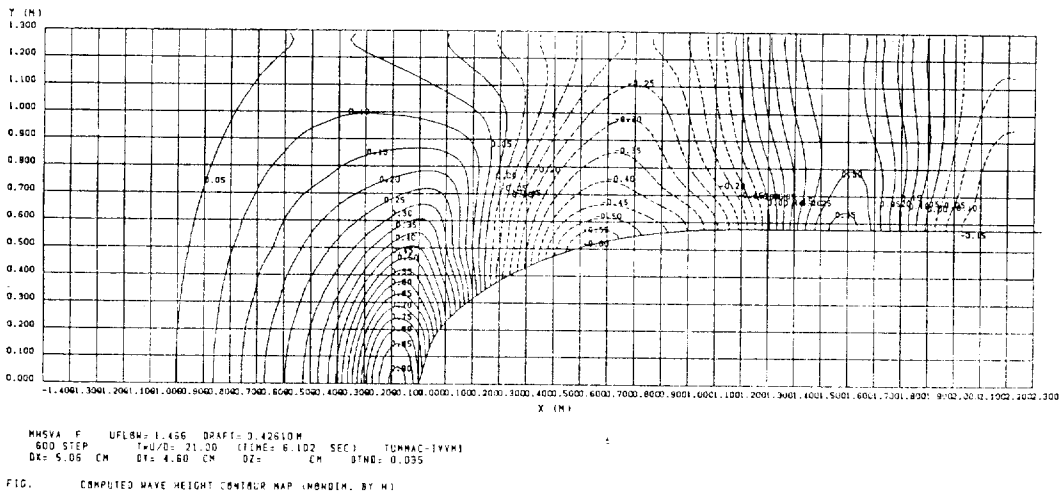

Fn = 0.17

Fig. 10 Wave-contour maps of the forebody of a HSVA model at Fn=0.15, 0.17, 600th time step

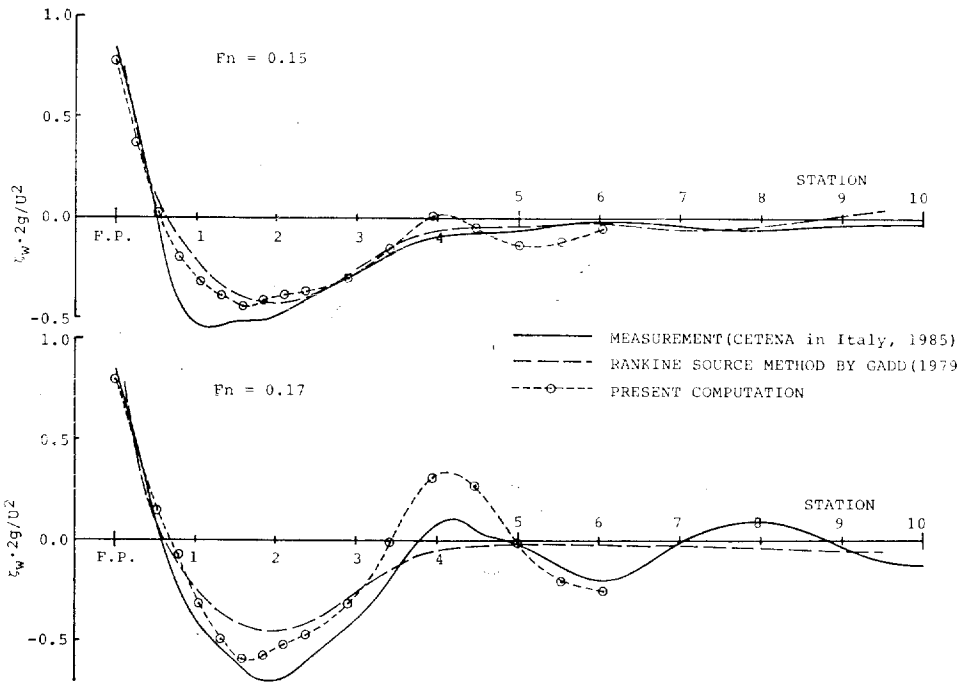

Fig. 11 Comparison of wave profiles on the hull surface of the forebody of a HSVA model at $Fn=0.15, 0.17$

at two points in the top and bottom cell of the inflow boundary is kept at the static pressure as standard values, and the pressure in other cells at $I=1$ is extrapolated from $I=2$ through the relation of the momentum equation. On the top and bottom boundaries the velocities are extrapolated so as to have no-normal-gradient of velocity on the boundaries. On the side open boundaries the periodic condition is imposed, and the no-normal-gradient condition is imposed for the outflow boundary. The marker-density is extrapolated with the same value from the fluid cells to the boundary cells.

4.2. Free-surface condition

In the previous studies, the Lagrangian movement of markers or segments are used for the implementation of the kinematic free-surface condition. However, these method seems to have serious difficulties when it is applied to the wave breaking with the overturning motion in three-dimensions. Therefore, a simple technique that uses marker-density is devised in this work.

It is assumed that the scalar variable of marker-

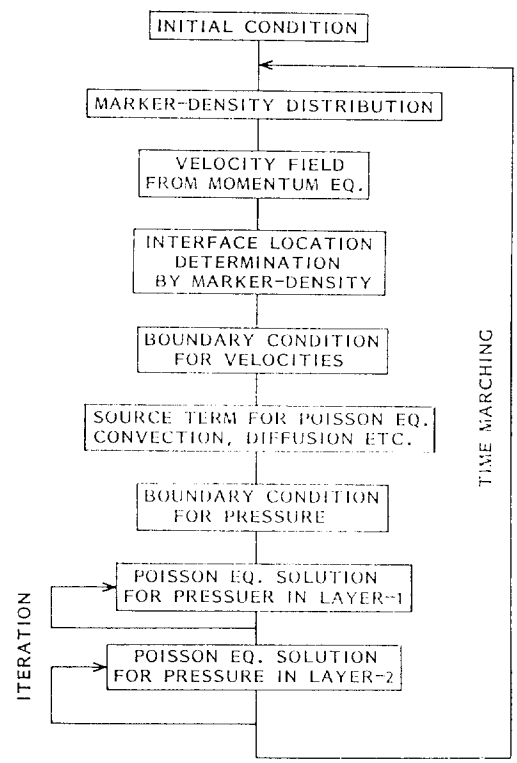

Fig. 12 Block diagram of the TUMMAC-VI scheme

density, that determines the free-surface location, is ruled by the equation of the kinematic free-surface condition as follows.

$$\frac{\partial \rho_m}{\partial t}+u\frac{\partial \rho_m}{\partial x}+v\frac{\partial \rho_m}{\partial y}+w\frac{\partial \rho_m}{\partial z}=0 \qquad (7)$$

Then, the location of the interface between two layers is determined by the following definition of the free-surface.

$$\rho_m=(\rho_m^1+\rho_m^2)/2 \qquad \text{on the interface} \quad (8)$$

Here, the superscripts 1, 2 imply the layer-1 and layer-2, respectively.

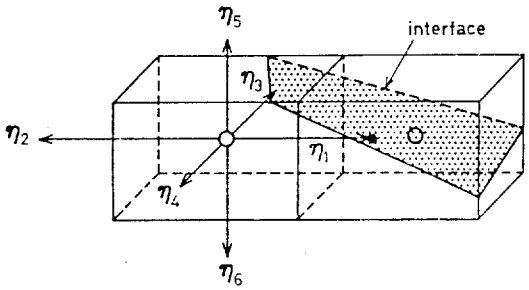

Fig. 13 The irregular star near the interface

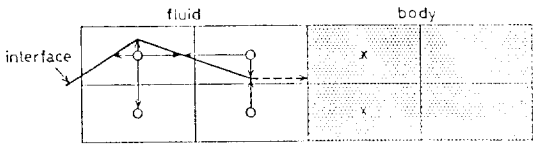

Fig. 14 Treatment of the interface locationat the intersection with an obstacle

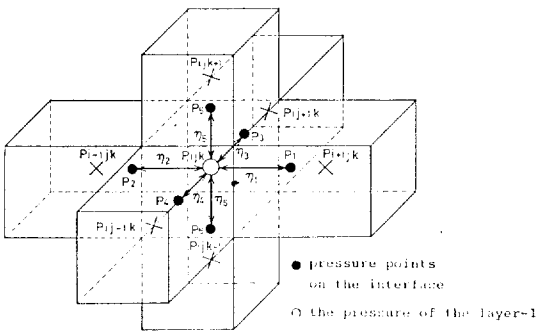

Fig. 15 Definition sketch for pressure extrapolation at the interface

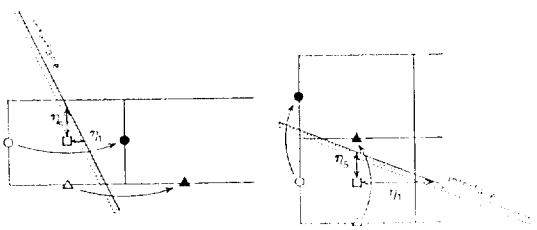

Fig. 16 Velocity extrapolation at the intercefa

Since the value of the marker-density is diffused across the interface in the course of the computation of the equation (7), this method obscures the interface location and the accuracy is inferior to the previous methods unless very fine grid spacing is used. It must be noted that the marker-density is used only for the determination of the interface location, and for the momentum and related equations two physical values of density are used.

The dynamic free-surface condition is satisfied by the so-called "irregular star" technique in the solution process for the Poisson equation. As shown in Fig. 13, the leg-length of the each irregular stars is calculated from the marker densities. At the intersection of the interface with the obstacle the slope of the interface is always assumed to be horizontal as shown in Fig. 14. This is to avoid singular behavior on this intersection.

The pressure on the interface is determined by extrapolating the pressure of the layer-1 to the inter-

Table 2 Condition of computation for a rectangular cylinder

Domain of computation (m) (length × width × depth)		0.60×0.46×0.64
Cell size (mm)	*DX*	10.0
	DY	10.0
	DZ	3.0~18.4
Approximate number of used cell		307800
Time increment *DT* (*s*)		0.0005
Time steps for acceleration		1000
Total time steps		1600
Relaxation factor ω		0.6
Density ρ (kg·sec²/m⁴) air/water		0.1229/101.79
Kinematic viscosity ν (m²/sec) air/water		1.502×10^{-5}/ 1.009×10^{-6}
Inflow condition air/water		0/uniflow
Uniflow velocity (m/s)		1.00
Fn		1.01

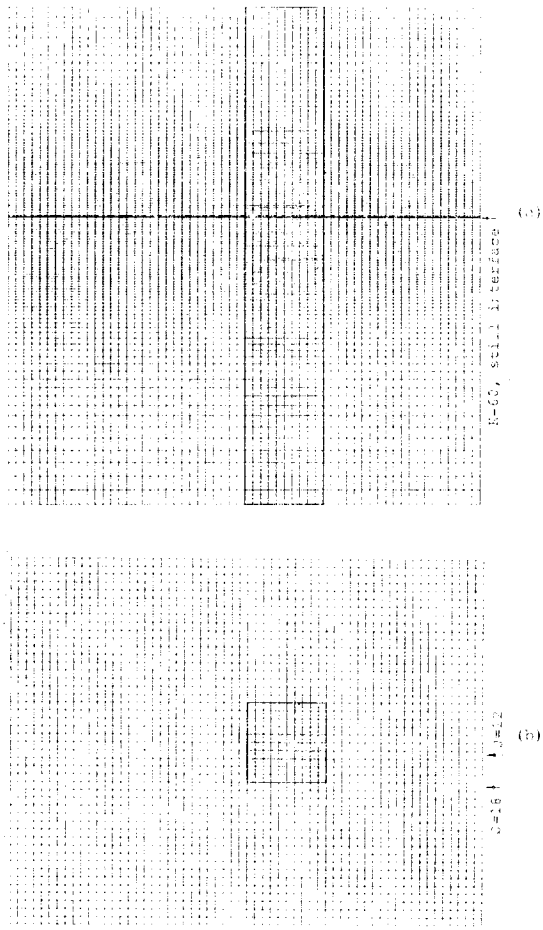

Fig. 17 Cell division of a rectangular cylinder,
(a) (x, z)-vertical and
(b) (x, y)-horizontal planes

face location as shown in Fig. 15. Precisely, the pressure on the interface is extrapolated as epuation (9).

$$P_1, P_2, P_3, P_4 = P_{i,j,k}$$
$$P_5 = P_{i,j,k} - \rho^1 g \eta_5$$
$$P_6 = P_{i,j,k} + \rho^1 g \eta_6 \quad (9)$$

The velocities near the interface are constantly extrapolated from the layer-2 to the layer-1 so that the velocity gradient in the normal direction approximately diminishes at the interface and consequently no unfavorable instability occur here. As shown in Fig. 16, they are horizontally extrapolated when the interface slope is greater than 45° or vertically otherwise.

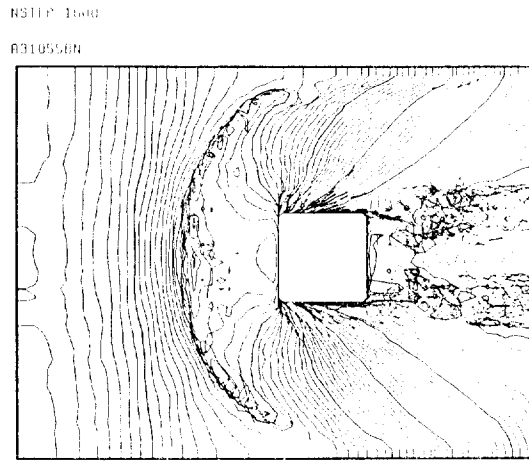

Fig. 18 Wave contour map of a rectangular cylinder at $U=1.0$m/s, 1,600 step(0.80sec)

5. Computed Results with TUMMAC-VI

5.1. Condition of computation

The grid system in the computational domain is shown in Fig. 17, and the conditions of computation are shown in Table 2.

The vertical rectangular cylinder piercing the interface of air and water has the horizontal cross-section of 0.1m×0.1m. The horizontal grid spacing DX and DY are uniformly 10mm all over the computational domain, and the vertical grid spacing $DZ(k)$ varies from 3mm to 18.4mm, namely the variable spacing is employed. The dimensions of the computational domain is 0.60m×0.46m×0.64m, and the total number of cell is 307,800.

The computation is started from the rest condition, and the fluid all over the computational domain is accelerated for 1,000 time steps. After the acceleration is finished, the computation is continued to the 1,600-th time step, the velocities at the inflow boundary being kept constant.

The Froude number based on the side length of the cylinder is 1.01.

5.2. Computed results

The wave contour map at 1,600-th time step (0.8 sec) is shown in Fig. 18. Since one contour curve is drawn in one horizontal layer of cells, this figure

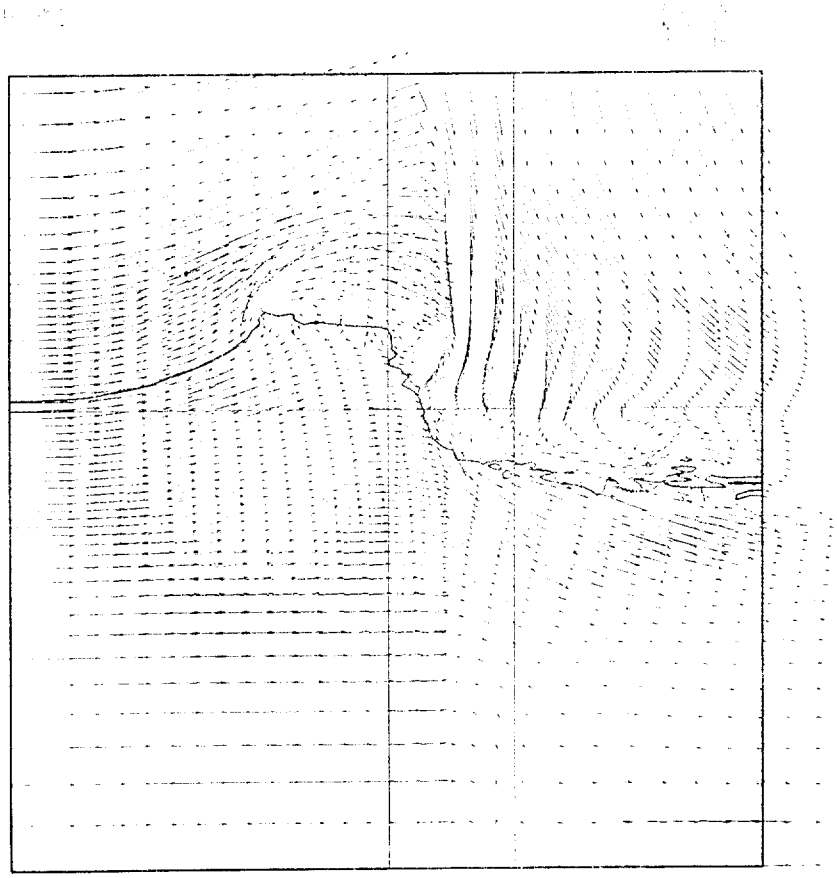

Fig. 19. Wave profile and velocity vector field of a rectangular cylinder on the vertical plane of $J=18$ at $U=1.0$m/s, 1,600 step (0.80sec)

gives only qualitative informations. However, it is clearly observed that a detached bow wave with circular plan-form is formed, and that another steep slope of the water surface appears from the forward corners of the cylinder. The complex wave breaking phenomena is also observed behind the cylinder. It will be safe to say that the wave formations in these simulated results show good resemblance to the physical phenomenon of strongly interacting interface.

The velocity vector field as well as the profile of the interface are shown on the vertical plane at $J=18$, as shown in Fig. 19. The vertical plane at $J=18$ is just on the side surface of the cylinder. The interpolated velocities at the pressure point of the cells are used for this figure, and the spacing between the starting points of the vectors is double of the grid spacing. The steep slope of the wave just behind the forward corners shows good agreement with the physical wave motions. The flow is separated at the sharp corners, and deeply suppressed region appears behind the cylinder, because very complicated flow-field of this region is involving vortical motion, free-surface turbulence, wave breaking and air-entrainment.

The contours of vertical velocity component w are shown on the vertical plane at $J=22$ in Fig. 20. The vertical plane at $J=22$ is almost on the center-plane of the cylinder. The intimate contours are concentrated near the strongly interacting interface, especially where wave breaking or air-entrainment takes place.

In Fig. 21, the velocity vector field and the inter-

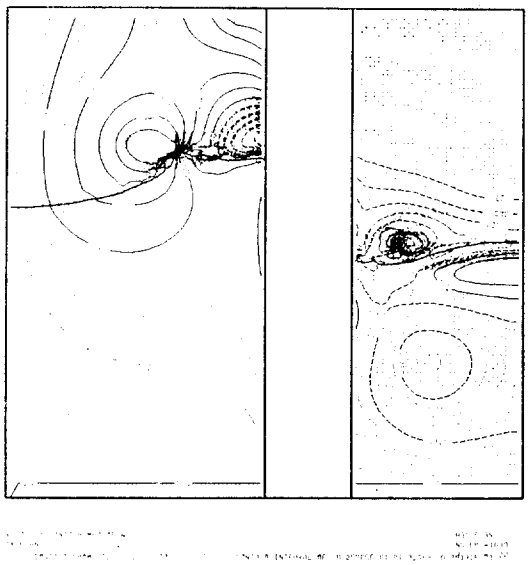

Fig. 20 Contour map of velocity component w of a rectangular cylinder on the vertical plane of $J=22$ at $U=1.0$m/s, 1,600 step (0.80sec)

face profile on a vertical plane ($I=29$) normal to the direction of the upstream flow are shown. The longitudinal location $I=29$ means the plane just before the cylinder. The front line of the detached bow wave is shown in this figure, and the vortex phenomenon appears in the air region above this front line.

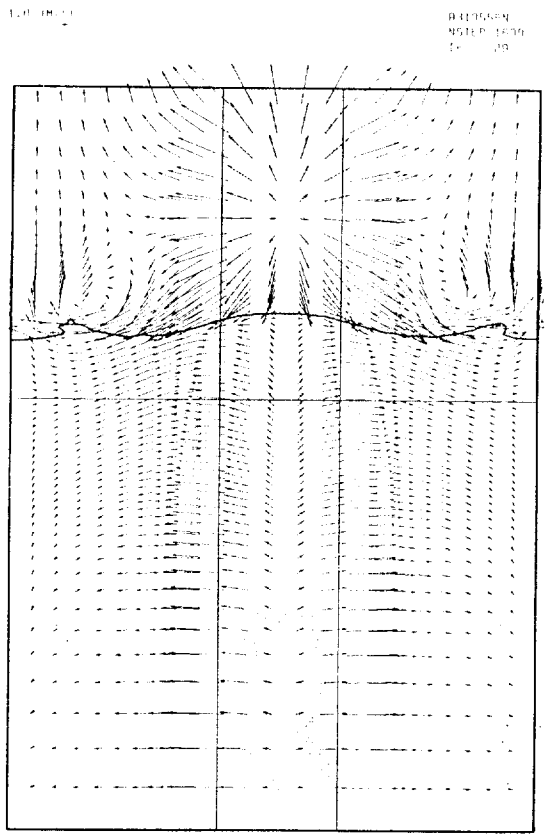

Fig. 21 Wave profile and velocity vector field of a rectangular cylinder on the vertical plane of $I=29$ at $U=1.0$m/s, 1,600 step (0.80sec)

6. Concluding Remarks

The simulations of the wave system about the full-length of a ship model are performed by the TUMMAC-IV$_{vm1}$ version with the improvement of the velocity extrapolation method in the B-cells of aft-body, the 3-dimensional exactness of relaxation factor ω_f and the improvement of free-surface treatment with the marker particles. In the comparison of computed and measured wave profiles along the hull surface, the agreement is satisfactory especially on the hull surface of the aft-body of the Series 60 hull. It may be considered that the influence of nonlinear free-surface effect is greater than the viscous effect in the wave pattern of the aft-body, because the Series 60 model is very thin. From the above results and the computational results of the bow waves around the HSVA model, TUMMAC-IV$_{vm1}$ method is ascertained to be effective for the simulation of nonlinear ship waves.

The wave breaking in a 3-dimensional space, which has been considered one of the most difficult problems for the numerical simulation of free-surface problem, is demonstrated to be resolved by the TUMMAC-VI method. Since the fluid motions of two layers are simultaneously simulated, it is considered that this method can be applied to a variety of two-layer problems. However, it is noted that the present method must be improved for the arbitrary body shape, etc.. Furthermore, because of the numerous approximations on the interface, computational accuracy is not sufficient in spite of the large

number of the grid points. The CPU time is more than fifteen hours for 1,600 time steps by the computer of the University of Tokyo HITAC M689/682H. These must be improved in future.

This research is partly supported by the Grant-in-Aid for Scientific Research of the Ministry of Education, Science and Culture, also partly by the LINEC group of shipbuilders in Japan.

References

[1] Miyata, H., "Characteristics of Nonlinear Waves in the Near-Field of Ships and Their Effects on Resistance", *Proc. 13th Sympo. Naval Hydrodynamics*, 1980.

[2] Miyata, H., et al., "Free Surface Shock Waves around Ships and Their Effects on Ship Resistance", *J. Soc. Naval Arch. Japan*, Vol. 147, 1980.

[3] Miyata, H., et al., "Numerical Explanation of Nonlinear Nondispersive Waves around Bow", *Proc. 3rd Intern. Conf. Numerical Ship Hydrodynamics*, Paris, 1981.

[4] Suzuki, A., et al., "Numerical Analysis of Free Surface Shock Waves around Bow by Modified MAC-Method (First Report)", *J. Soc. Naval Arch. Japan*, Vol. 150, 1981.

[5] Masuko, A., et al., "Numerical Analysis of Free Surface Shock Waves around Bow by Modified MAC-Method (Second Report)", *J. Soc. Naval Arch. Japan*, Vol. 152, 1982.

[6] Aoki, K., et al., "Numerical Analysis of Free Surface Shock Waves around Bow by Modified MAC-Method (Third Report)", *J. Soc. Naval Arch. Japan*, Vol. 153, 1983.

[7] Aoki, K., et al., "A Numerical Analysis of Nonlinear Waves Generated by Ships of Arbitrary Waterline (First Report)", *J. Soc. Naval Arch. Japan*, Vol. 154, 1983.

[8] Miyata, H., et al., "A Numerical Analysis of Nonlinear Waves Generated by Ships of Arbitrary Waterline (Second Report)", *J. Soc. Naval Arch. Japan*, Vol. 155, 1984.

[9] Miyata, H., et al., "Finite-Difference Simulation of Nonlinear Ship Waves", *J. Fluid Mech.*, Vol. 157, pp. 327-357, 1985.

[10] Nishimura, S., et al., "Finite-Difference Simulation of Ship Waves by the TUMMAC-IV Method and Its Application to Hull-Form Design", *J. Soc. Naval Arch. Japan*, Vol. 157, pp. 1-14, 1985.

[11] Welch, J.E., et al., "The MAC Method", Los Alamos Scientific Lab. Report LA-3425, Los Alamos, New Mexico, 1966.

[12] Miyata, H., "Finite-Difference Simulation of Breaking Waves", *J. Computational Phys.*, 65, pp. 179-214, 1986.

[13] Katsumata, M., "A Finite-Difference Simulation of Two-Layer Flow (about the Application for 3-Dimensional Wave-Breaking Problem)", Master thesis, the University of Tokyo, March, 1987.

[14] Hirt, C.W. et al., "Volume of Fluid (VOF) Method for the Dynamics of Free Boundaries", *J. Computational Phys.*, 39, 1981.

[15] Chan, R.K.-C. & Street, R.L., "A Computer Study of Finite-Amplitude Water Waves", *J. Computational Phys.*, 6, pp. 68-94, 1970.